PCCP

PAPER

View Article Online
View Journal | View Issue

Cite this: *Phys. Chem. Chem. Phys.*, 2017, **19**, 26164

Electronic excitation induced hydrogen-bond adjustment and lattice control in organic–inorganic hybrid cubic perovskites: a fixed occupation molecular dynamics study†

Mo-Ran Wang,[a] Xiang-Yang Ren,[a] Xian-Bin Li,*[ab] Nian-Ke Chen[a] and Hong-Bo Sun[a]

Received 25th July 2017,
Accepted 1st September 2017

DOI: 10.1039/c7cp05034h

rsc.li/pccp

The organic–inorganic hybrid perovskite has become a new type of semiconductor for low cost and highly efficient solar cells. However, the mechanism of interactions between the organic cation and the inorganic framework is still not completely clear under optical electronic excitation. In this work, we employ first-principles molecular dynamics with electronic excitation effects to prove that the hydrogen-bond interaction between the molecular cation and the inorganic lattice can be readily adjusted by several-percentage-valence-electron excitations in cubic $CH_3NH_3PbI_3$. While the hydrogen-bond interaction causes serious lattice distortions, the electronic excitation can recover the lattice symmetry largely by weakening hydrogen bonding. The study offers atomic dynamics to understand the excitation process in the organic–inorganic hybrid perovskite semiconductor.

Introduction

Organic–inorganic hybrid perovskites (OIHP) have attracted significant attention because of the excellent optical performance, the simple fabrication, and the low cost for optoelectronic devices.[1–3] They can be obtained *via* annealing at low temperature (about 100 °C) after spin coating.[4] On the other hand, theirs excellent properties include the low recombination rate, the long carrier-diffusion length, and the suitable direct band gap for absorption of solar light.[5–8] As such, the OIHP have been employed in solar cells,[9] photodetectors,[10] LASER,[11] and light-emitting devices.[12] Among them, the solar cell is the main hotspot. In 2009, Miyasaka *et al.* first applied $MAPbX_3$ (X = I, Br; MA is short for CH_3NH_3) in dye-sensitized solar cells with a power conversion efficiency (PCE) of 3.8%.[13] In 2011, Park *et al.* improved the PCE to 6.5% by using $MAPbI_3$ nanoparticles on TiO_2 and iodide/iodine redox electrolytes.[14] In the past several years, the efficiency of the perovskite solar cells has increased over 20%.[15] Most recently (2017), a Perovskite-Silicon Tandem Solar Cell has been reported with over 26% PCE, which is very close to the current record for a single junction silicon cell of 26.6%.[16]

With the rapid development of applications in solar cells, the perovskite structures have been widely studied. They usually have the composition of ABX_3, where A^+ can be for example $CH_3NH_3^+$ (MA^+), $NH_2CHNH_2^+$ (FA^+), Cs^+; B can be Pb or Sn[17] and X can be Cl, Br, I or their mixture.[18] Here, for the most popular $MAPbI_3$, X-ray diffraction experiments showed that phase change occurs at 162 K and 327 K along with the change of MA orientation. When the temperature is below 160 K, $MAPbI_3$ is orthorhombic. At 162 K, its structure is changed from the orthorhombic phase to the tetragonal phase while at 327 K it is changed from the tetragonal phase to the cubic phase.[19] Zhang *et al.* have studied the photovoltaic performances of $MAPbI_3$ in these temperature ranges and showed that the photovoltaic properties, especially the short circuit and the fill factor, did not change considerably from the tetragonal to cubic phase. However, the PCE is significantly reduced when the structure is changed to the orthorhombic structure.[20]

Although significant progress has been made for hybrid perovskites, there are still some fundamental problems that need to be further illustrated. One of these is the role of organic molecular cations in the inorganic lattice. In fact, OIHP may be considered as another kind of semiconductor which is different from the pure inorganic semiconductor or the pure organic semiconductor. Static density functional theory calculations for band structures and density of states has shown that the electronic states of organic molecules do not belong to the band-edge states in OIHP.[21] Naively, we may conclude that organic molecules may not be involved in optical processes,

[a] *State Key Laboratory on Integrated Optoelectronics, College of Electronic Science and Engineering, Jilin University, Changchun 130012, China. E-mail: lixianbin@jlu.edu.cn*
[b] *Lab of Computational Semiconductor Physics, Jilin University, Changchun 130012, China. Web: www.ioe-jlu.cn/csp*

† Electronic supplementary information (ESI) available. See DOI: 10.1039/c7cp05034h

such as optical excitation process in practical applications. However, at different temperatures, such organic cations have been proposed to display different motion patterns. At low temperature (<162 K), the MA cation has been proposed as an order arrangement in the $MAPbI_3$ orthorhombic phase. At room temperature, MA cations show 2D-disorder motion in the tetragonal phase. However, at a relatively high temperature (>327 K), MA exhibits 3D-disorder rotation in the cubic phase[22] where the organic molecules have different orientations and possibly have influences on band edge states *via* adjusting the inorganic lattice. For example, when the orientation of organic molecules is changed from [111] to [011] in the cubic phase, the band gap will be changed from a direct band gap to an indirect band gap.[23] On the other hand, the hydrogen-bond interaction between the halogen atoms and organic cations can cause a certain degree of tilting of the PbI_6 octahedron. In other words, organic molecules in the perovskite could indirectly affect the band structure and optical performance through their motions or hydrogen bond (HB) interaction. Therefore, how to control the pattern of organic cations in OIHP is worth studying.

In this work, we carried out density functional theory (DFT) molecular dynamics studies with the fixed-occupation method to evaluate the electronic excitation effects in cubic perovskite $MAPbI_3$. Although excitation disturbed electrons are not directly linked to MA cations, the significant impact on HB between MA and I is identified by analyses of atomic motions. In the ground state, the HBs are strong enough to distort the lattice with the manifestation of the averaged Pb–I–Pb bond angle of 148°, not the ideal 180°. With a certain electronic excitation, such as a 2.88% valence electron, the HB interactions are obviously suppressed and the inorganic lattice can largely recover their cubic symmetry. The present study offers an updated insight into optical physics process for OIHP materials.

Method

The studies are carried out by first-principles calculations based on density functional theory implemented in the VASP code.[24,25] The generalized-gradient-approximation Perdew–Burke–Ernzerhof (GGA-PBE) functional[26] is used to evaluate the exchange–correlation interaction. The energy cutoff for planewave expansion is 480 eV. A 2 × 2 × 2 cubic $MAPbI_3$ supercell with 96 atoms is used in the molecular dynamics (MD) study. In the MD simulation, we use the canonical *NVT* ensemble, in which the Nose–Hoover thermostat is used to control the temperature.[27] To mimic optical excitation induced electrons transition at band edges, a fix occupation method is employed.[28] The MD time step is 1 fs. In order to test the reasonability of the time step, a 0.1 fs is also used and the results are consistent with the ones of the 1 fs time step. The *K*-point mesh grid for Brillouin zone integration are 7 × 7 × 7 and 1 × 1 × 1 for static self-consistent calculations and MDs, respectively. All atoms are relaxed until the Hellmann–Feynman forces on individual atoms are less than 0.01 eV $Å^{-1}$. The effect of spin–orbit coupling (SOC) is not considered. Periodic boundary conditions are used in all of our calculations.

Results and discussion

Before the discussion on electronic excitation in $MAPbI_3$, its structure is briefly described. Fig. 1a shows the static cubic model where corner-sharing PbI_6 octahedra construct the inorganic cubic framework. Molecular MA groups act as a −1 charged cation, sitting at the center of the Pb cubic framework. This kind of structure indicates a significant electronic characteristic, *i.e.* the cross-gap hybridization[29] where the states of anion I contribute to the valence band while the states of cation Pb contribute to the conduction band, see the electronic density of states (DOS) in Fig. 1b. Interestingly, MA molecular cations contribute little to both the band edges which indicate they "cannot" take part in a photon induced electronic transition. These results are also consistent with the previous band structure and DOS studies.[23,30–32] Fig. 1c (charge density difference between a 2.88% excitation state and its ground state) further demonstrates the trend of electron redistribution from I to Pb after the excitation transition. Once again, this is not related to any MA cations. Here, the red color indicates electron accumulation, blue color indicates hole accumulation, and the green color indicates no significant change.

Based on the discussion above, MA cations should play the smallest role in the excitation of OIHPs. Under actual conditions, MA cations are in the form of a highly mobile state due to the lack of strong chemical bonding (like covalent or ionic bonding) with the inorganic framework. In order to identify the role of MA, we carry out first-principles molecular dynamics at 330 K at which the cubic phase exists.[33] It is known that

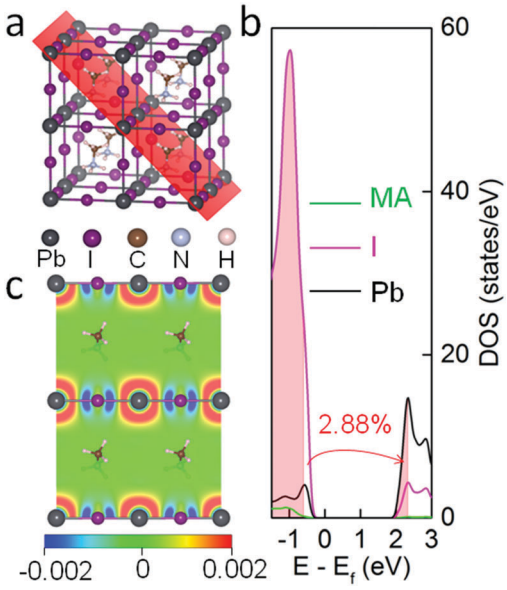

Fig. 1 (a) 2 × 2 × 2 cubic $CH_3NH_3PbI_3$ model for this study. (b) Local density of states in the $MAPbI_3$ model where 2.88% of the valance electrons is displayed to be excited from VBM to CBM. (c) Charge density difference between the excitation state and its ground state in a plane which is sliced in the model (a).

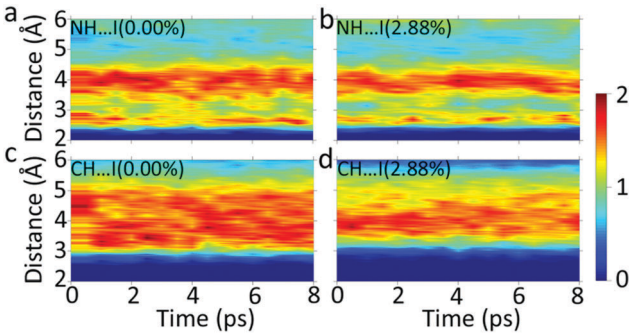

Fig. 2 The evolution of pair correlation function (PCF) between hydrogen and iodine in hydrogen bond of NH···I (a) and CH···I (c) in the ground state and those of NH···I (b) and CH···I (d) in the 2.88% excitation state. The cutoff of atomic distance is set to 6 Å. The intensity of PCF is displayed by the color bar.

hydrogen atoms are composed of the outmost shell of the MA cation. These are directional "hands" to touch the inorganic framework. Thus, we plot the time-dependent pair correlation function (PCF) between the hydrogen atoms of MA and the negatively charged I atoms. We also separate the PCFs into two cases: one is from the carbon bonded hydrogen (CH) while the other is from the nitrogen bonded hydrogen (NH). Fig. 2 shows the results. In the ground state, the PCFs of NH···I are discontinued and divided into two parts according to the distance between H and I: the shorter one (2.5–3 Å) and the longer one (3.5–4.5 Å), see Fig. 2a. In contrast, the PCFs of CH···I are longer in distance and continue from 3–5 Å, see Fig. 2c. These directly reflect the HB interaction between H and I. The hierarchical interaction for NH···I indicates its stronger bonding than that of CH···I. This is because the electronegativity of N atoms (3.04) is larger than that of C atoms (2.55) according to the Pauling scale.[34] H atoms are strongly connected with N atoms rather than C atoms. As such, the N-bonded H is more positively charged to form a stronger hydrogen bonding with I atoms. The longer distance in both cases and the broad continuing distribution in CH···I imply random rotations of MA cations in the inorganic framework. Therefore, the MA cations can play a role in the lattice *via* hydrogen bonding even if their electronic states do not matter with the band edges.

According to the discussion above, electronic excitation is a possible route to control hydrogen bonding between MA and I due to a reduction of I electrons in such a case. To demonstrate this idea, another 8 ps molecular dynamics simulation employs a condition with a 2.88% excitation in cubic $MAPbI_3$ at 330 K. Fig. 2b and d show their time dependent PCFs. It is noted that both the distances of CH···I or NH···I are elongated after excitation. But the form of PCF is similar to that in the ground state, *i.e.* the NH···I shows a discontinued style and the CH···I shows a continued style. In order to view the situation in the excitation clearly, the differences of PCF between the 2.88% excitation state and the ground state are analyzed in Fig. 3. This is defined as [PCF (excitation)–PCF (ground state)]. Here, the blue trough along the distance represents the decrease of the H···I distribution while the red peak along the distance represents the increase of the distribution. Both for NH···I and CH···I, the first trough occurs at the shortest H···I distance. With increasing the distance, some peaks appear. In other words, the original strongest HBs are suppressed and the other HBs become longer after excitation. Here, we also find that the differences of PCF are fluctuating rather than constant, especially for the 4 Å CH···I bonding. We interpret this phenomenon as a result of thermal fluctuations. Despite the fluctuations at this longer distance, the nearest trough basically remained unchanged. In other words, a conclusion of weakening hydrogen bonds under excitation should be made. Here, we further see that the change of the CH···I distribution is more obvious than that of the NH···I distribution. We consider this should be due to the original contrast in strength between NH···I and CH···I. In sum, the HB is significantly weakened and thus can be controlled by electronic excitation.

Next, Fig. 4 shows the results of the lattice under excitations. We define a physical quantity $\overline{\delta^2}(t)$ below, which indicates the bond-length (BL) variance of HB between an I atom and its four MA neighbors.

$$\overline{\delta^2}(t) = \frac{1}{24} \times \sum_{i=1}^{24} \left(\frac{1}{4} \times \sum_{j=1}^{4} \left(d_{ij}^{\min}(t) - \overline{d_{ij}^{\min}}(t) \right)^2 \right) \quad (1)$$

Here, the BL chooses the shortest one among the six distances of H···I in an MA cation at every moment, $d_{ij}^{\min}(t)$. In the

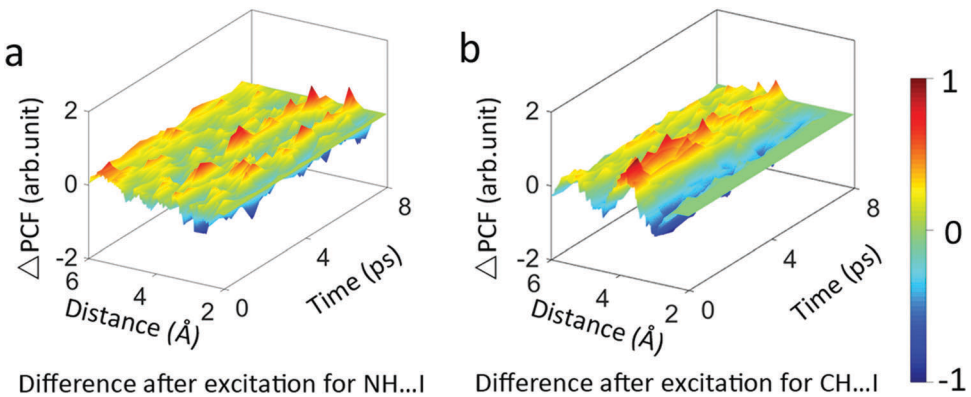

Fig. 3 The difference of PCFs [PCF (excitation)–PCF (ground state)] for NH···I (a) and CH···I (b). A color bar shows the change of intensity. Red color indicates the excitation enhancing PCF and blue color stands for the excitation weakening PCF. The excitation is 2.88%.

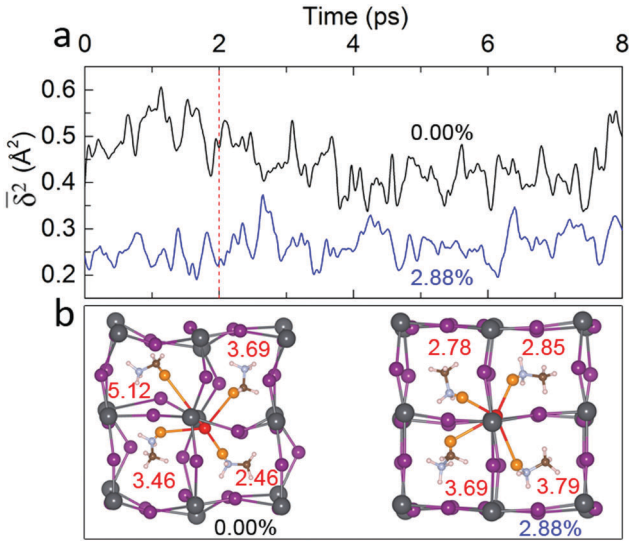

Fig. 4 (a) The variance distribution of correlated hydrogen-bonding bond lengths between each iodine and its four nearest MAs with or without excitation. (b) Two typical snapshots (at 2 ps) with/without excitation. In the ground state, the relatively strong hydrogen bond (with BL = 2.46 Å) causes iodine atom displaced while excitation weakens the interaction, thus making the displacement obviously weakened. Here, the described I atom and H atoms are highlighted with red and orange color, respectively. The four HB-BLs are shown next to the highlighted MA.

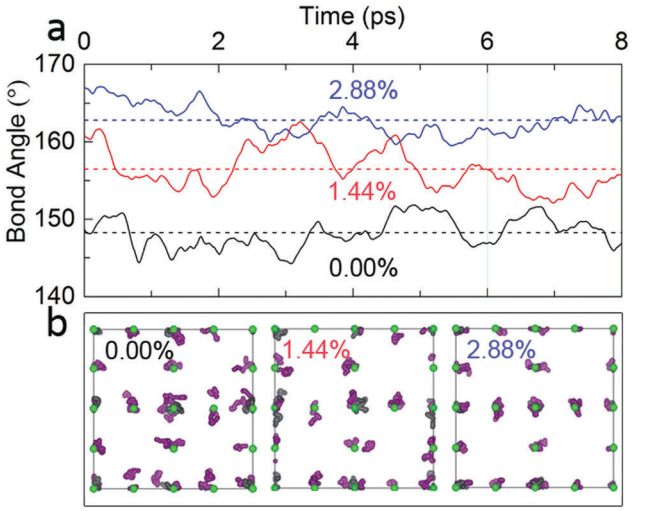

Fig. 5 (a) Time evolution of Pb–I–Pb bond angles reflecting the distortion degree of inorganic frameworks under different excitation intensities. (b) The (001) plane projected trajectory of inorganic atoms from 6–8 ps (shadowed by green color). Here, the green balls are for the referred positions in a standard cubic perovskite structure.

calculated supercell, i is for the 24 I anions and j is for the 4 neighboring MA cations for a certain I. As such, $\overline{\delta^2}(t)$ reflects the fluctuation of HB-BL. From Fig. 4a, it is very clear that the fluctuation of HB-BL at the ground state is two times larger than that of the excitation state. This is because the weakened interactions between I and MA under excitation can lower the displacement of I from its original lattice. As a result, the HB-BL is closer and the degree of structural distortion is reduced. For example, Fig. 4(b) shows typical snapshots (at 2 ps) with and without excitation.

In the ground state, the four HB-BLs around a highlighted I (indicated by red color) are 5.12 Å, 3.69 Å, 3.46 Å, 2.46 Å where a special short (strong) HB (BL = 2.46 Å) can be seen. This strong HB drags the I atom significantly off the ideal position towards to the corresponding MA. At the same time, a very long (weak) HB (BL = 5.12 Å) can be also observed on the opposite direction. In contrast, in the excitation state, the BLs of HBs for the highlighted I are less fluctuated, *i.e.* 3.79 Å, 3.69 Å, 2.85 Å, and 2.78 Å. No obvious distortion of the highlighted I is off the ideal lattice.

Finally, we observe the impact on the global lattice induced by excitations. Fig. 5a displays the evolution of the global lattice *via* the Pb–I–Pb angle which should be perfectly 180° in the static cubic structure. However, due to the existence of relatively strong HB in the ground state, the global lattice is not ideal but really distorted, as manifested by the averaged 148° Pb–I–Pb bond angle which is 18% less than the ideal 180°. However, when the excitation increases to 1.44%, and to 2.88% from the ground state, the bond angle is also gradually close to the ideal value, *i.e.* 148° (0%), 157° (1.44%), and 163° (2.88%). Here, more direct evidence for the change of global inorganic lattice is given in Fig. 5b, hiding all the MAs for easy observation. We display the ideal position of the inorganic lattice (with green balls) for reference and the realistic trajectory of atoms over 6–8 ps. In the ground state, a large discrepancy from the ideal position is clearly seen while with excitation the inorganic atoms are restored largely to the cubic lattice. All of these are consistent with the explanation of HB weakening by excitation and thus adjustment of the inorganic lattice in $MAPbI_3$. A video about "Excitation Impact on Lattice" can be seen in the supporting document "V1".

Conclusion and outlook

In this study, through first-principles calculations we evaluate the role of electronic excitation[35,36] in the interaction between organic cations and the inorganic framework of $MAPbI_3$. In the ground state, the inorganic lattice is distorted seriously from the ideal cubic perovskite lattice due to relatively strong HB between MA and I. However, after excitation, the HB is significantly weakened. As a result, the inorganic framework can be recovered largely due to the standard cubic lattice. The present study may offer an updated insight on the molecule-atom interacting mechanism under optical excitation from the dynamics, which may help understand the optical physics process in organic–inorganic hybrid systems and improve the performance of their optical absorption devices.

Conflicts of interest

There are no conflicts to declare.

Acknowledgements

This work was supported by the National Natural Science Foundation of China (NSFC) and National Key Research and

Development Program under Grants #11374119, #2017YFB1104300, #61590930, #91423102, #21473076 and 973 Program (No. 2014CB921303). The high-performance computing center (HPCC) of Jilin University is also acknowledged for the calculation resources.

Notes and references

1 H. J. Snaith, *J. Phys. Chem. Lett.*, 2013, **4**, 3623–3630.
2 H. Fang, S. Adjokatse, N. Zhao, J. Even and M. A. Loi, *Light: Sci. Appl.*, 2016, **5**, e16056.
3 Y. Zhao, W. Zhou, X. Zhou, K. Liu, D. Yu and Q. Zhao, *Light: Sci. Appl.*, 2017, **6**, e16243.
4 T. J. Jacobsson, W. Tress, C.-B. Juan-Pablo, T. Edvinsson and A. Hagfeld, *J. Phys. Chem. C*, 2016, **120**, 11382–11393.
5 H. Oga, A. Saeki, Y. Ogomi, S. Hayase and S. Seki, *J. Am. Chem. Soc.*, 2014, **136**, 13818–13825.
6 S. D. Stranks, G. E. Eperon, G. Grancini, C. Menelaou, M. J. P. Alcocer, T. Leijtens, L. M. Herz, A. Petrozza and H. J. Snaith, *Science*, 2013, **342**, 341–344.
7 G. Xing, N. Mathews, S. Sun, S. S. Lim, Y. M. Lam, M. Grätzel, S. Mhaisalkar and T. C. Sum, *Science*, 2013, **342**, 344–347.
8 S. D. Wolf, J. Holovsky, S. J. Moon, P. Loper, B. Niesen, M. Ledinsky, F. J. Haug, J. H. Yum and C. Ballif, *J. Phys. Chem. Lett.*, 2014, **5**, 1035–1039.
9 D. P. McMeekin, G. Sadoughi, W. Rehman, G. E. Eperon, M. Saliba, M. T. Horantner, A. Haghighirad, N. Sakai, L. Korte, B. Rech, M. B. Johnston, L. M. Herz and H. J. Snaith, *Science*, 2016, **351**, 151.
10 K. Domanski, W. Tress, T. Moehl, M. Saliba, M. K. Nazeeruddin and M. Gratzel, *Adv. Funct. Mater.*, 2015, **25**, 6936–6947.
11 F. Deschler, M. Price, S. Pathak, L. E. Klintberg, D. D. Jarausch, R. Higler, S. Huttner, T. Leijtens, S. D. Stranks, H. J. Snaith, M. Atature, R. T. Phillips and R. H. Friend, *J. Phys. Chem. Lett.*, 2014, **5**, 1421.
12 L. C. Schmidt, A. Pertegás, S. González-Carrero, O. Malinkiewicz, S. Agouram, G. M. Espallargas, H. J. Bolink, R. E. Galian and J. Pérez-Prieto, *J. Am. Chem. Soc.*, 2014, **136**, 850.
13 A. Kojima, K. Teshima, Y. Shirai and T. Miyasaka, *J. Am. Chem. Soc.*, 2009, **131**, 6050–6051.
14 J.-H. Im, C.-R. Lee, J.-W. Lee, S.-W. Park and N.-G. Park, *Nanoscale*, 2011, **3**, 4088–4093.
15 Efficiency Chart, https://www.nrel.gov/pv/assets/images/efficiency-chart.png, 2017.
16 T. Duong, Y. Wu, H. Shen, J. Peng, X. Fu, D. Jacobs, E. Wang, T. C. Kho, K. C. Fong, M. Stocks, E. Franklin, A. Blakers, N. Zin, K. McIntosh, W. Li, Y. Cheng, T. P. White, K. Weber and K. Catchpole, *Adv. Energy Mater.*, 2017, **7**, 1700228.
17 C. C. Stoumpos, C. D. Malliakas and M. G. Kanatzidis, *Inorg. Chem.*, 2013, **15**, 9019–9038.
18 O. Selig, A. Sadhanala, C. Muller, R. Lovrincic, Z. Chen, Y. L. A. Rezus, J. M. Frost, T. L. C. Jansen and A. A. Bakulin, *J. Am. Chem. Soc.*, 2017, **139**, 4068–4074.
19 M. T. Weller, O. J. Weber, P. F. Henry, A. M. Di Pumpo and T. C. Hansen, *Chem. Commun.*, 2015, **51**, 4180–4183.
20 H. Zhang, X. Qiao, Y. Shen, T. Moehl, S. Zakeeruddin, M. Gratzel and M. Wang, *J. Mater. Chem. A*, 2015, **3**, 11762–11767.
21 E. Menendez-Proupin, P. Palacios, P. Wahnon and J. C. Conesa, *Phys. Rev. B: Condens. Matter Mater. Phys.*, 2014, **90**, 045207.
22 J. M. Frost and A. Walsh, *Acc. Chem. Res.*, 2016, **49**, 528–535.
23 C. Motta, F. El Mellouhi, S. Kais, N. Tabet, F. Alharbi and S. Sanvito, *Nat. Commun.*, 2015, **6**, 7026.
24 G. Kresse and J. Furthmuller, *J. Comput. Mater. Sci.*, 1996, **6**, 15.
25 G. Kresse and J. Furthmuller, *Phys. Rev. B: Condens. Matter Mater. Phys.*, 1996, **54**, 11169.
26 J. P. Perdew, K. Burke and M. Ernzerhof, *Phys. Rev. Lett.*, 1996, **77**, 3865.
27 S. Nose, *J. Chem. Phys.*, 1984, **81**, 511–519.
28 P. Tangney and S. Fahy, *Phys. Rev. B: Condens. Matter Mater. Phys.*, 2002, **65**, 054302.
29 S. Mukhopadhyay, J. Sun, A. Subedi, T. Siegrist and D. J. Singh, *Sci. Rep.*, 2016, **6**, 25981.
30 T. Baikie, Y. Fang, J. M. Kadro, M. Schreyer, F. Wei, S. G. Mhaisalkar, M. Graetzeld and T. J. White, *J. Mater. Chem. A*, 2013, **1**, 5628–5641.
31 F. Brivio, K. T. Butler and A. Walsh, *Phys. Rev. B: Condens. Matter Mater. Phys.*, 2014, **89**, 155204.
32 P. Umari, E. Mosconi and F. D. Angelis, *Sci. Rep.*, 2014, **4**, 4467.
33 F. Brivio, J. M. Frost, J. M. Skelton, A. J. Jackson, O. J. Weber, M. T. Weller, A. R. Goni, A. M. A. Leguy, P. R. F. Barnes and A. Walsh, *Phys. Rev. B: Condens. Matter Mater. Phys.*, 2015, **92**, 144308.
34 A. L. Allred, *J. Inorg. Nucl. Chem.*, 1961, **17**, 215–221.
35 X.-B. Li, X. Q. Liu, D. Han, Z. Zhang, X. D. Han, H.-B. Sun and S. B. Zhang, *Phys. Rev. Lett.*, 2011, **107**, 015501.
36 N.-K. Chen, D. Han, X.-B. Li, F. Liu, J. Bang, X.-P. Wang, Q.-D. Chen, H.-Y. Wang, S. B. Zhang and H.-B. Sun, *Phys. Chem. Chem. Phys.*, 2017, DOI: 10.1039/C7CP03103C.

